Journal of Hazardous Materials 419 (2021) 126458

Contents lists available at ScienceDirect

Journal of Hazardous Materials

journal homepage: www.elsevier.com/locate/jhazmat

Electrochemical reductive remediation of trichloroethylene contaminated groundwater using biomimetic iron-nitrogen-doped carbon

Jia Deng [a], Xin-Ming Hu [b], Enlai Gao [a], Feng Wu [c], Weizhao Yin [d], Li-Zhi Huang [a,e,*], Dionysios D. Dionysiou [f]

[a] School of Civil Engineering, Wuhan University, No. 8, East Lake South Road, Wuhan, PR China
[b] Environment Research Institute, Shandong University, Qingdao 266237, PR China
[c] School of Resources and Environmental Science, Wuhan University, Wuhan, PR China
[d] School of Environment, Jinan University, Guangzhou 510632, PR China
[e] State Key Laboratory of Water Resources and Hydropower Engineering Science, Wuhan University, 430072, PR China
[f] Environmental Engineering and Science Program, Department of Chemical and Environmental Engineering, University of Cincinnati, Cincinnati, Ohio 45221-0012, United States

ARTICLE INFO

Editor: Dr. Danmeng Shuai

Keywords:
Reductive dechlorination
Trichloroethylene
Groundwater remediation
FeNC catalyst
Biomimetic catalyst

ABSTRACT

Electrochemical dechlorination is a prospective strategy to remediate trichloroethylene (TCE)-contaminated groundwater. In this work, iron-nitrogen-doped carbon (FeNC) mimicking microbiological dechlorination co-enzymes was developed for TCE removal under environmentally related conditions. The biomimetic FeNC-900, FeNC-1000, and FeNC-1100 materials were synthesized via pyrolysis at different temperatures (900, 1000, and 1100 °C). Due to the synergistic effect of Fe–N_4 active sites and graphitic N sites, FeNC-1000 had the highest electron transfer efficiency and the largest electrochemical active surface area among the as-synthesized FeNC catalysts. The pseudo-first-order rate constants for TCE reduction using FeNC-1000 catalyst are 0.19, 0.28 and 0.36 h^{-1} at potentials of −0.8 V, −1.0 V and −1.2 V, respectively. Active hydrogen and direct electrons transfer both contribute to the dechlorination from TCE to C_2H_4 and C_2H_6. FeNC maintain a high reactivity after five reuse cycles. Our study provides a novel approach for the dechlorination of chlorinated organic contaminants in groundwater.

1. Introduction

With the acceleration of industrialization and rapid population growth, groundwater pollution has become a serious global problem (Murakami et al., 2009; He et al., 2019). Trichloroethylene (TCE), as one of the most widely used chlorinated organic solvents, is frequently detected in groundwater (Westrick et al., 1984; Moran et al., 2007). Due to the strong migration ability and carcinogenicity, TCE contamination brings serious hazardous effect to human (Smith et al., 1996; Press et al., 2016). Thus, exploring efficient and applicable technology for the remediation of TCE contaminated groundwater is imperative (Li et al., 2004; Yin et al., 2020).

In recent years, electrochemistry processes targeting the degradation of soluble refractory pollutants in groundwater have been intensively investigated (Miao et al., 2009; Prasad and Srivastava, 2009; Huang et al., 2015). Electrochemical methods show excellent dehalogenation and detoxification capability to halogenated organic pollutants (HOPs) (Schaefer et al., 2018; Yin et al., 2020). Electrochemical cathodes can provide sufficient electrons to HOPs for reductive dehalogenation (Antonello and Maran, 1999; Van Hoomissen and Vyas, 2019). Also, some researchers developed catalyst-loaded cathode which generated active hydrogen (H*) to attack halogenated groups for detoxification (Mao et al., 2019; Zhang et al., 2019). According to previous studies, direct electrochemical reduction of TCE at a cathode favor the formation of chloroacetylene at a standard reduction potential of −2.276 V vs. saturated calomel electrode (SCE) (Lei et al., 2019). For the direct electrochemical reduction of TCE, hydrodechlorination and reductive β−elimination take place simultaneously. The complete dechlorination product is acetylene, of which the standard reduction potential is close to −3.0 V vs. SCE (Durante et al., 2013). However, direct electrochemical reduction of TCE in groundwater remains a challenge due to the problems caused by high energy consumption and low

* Corresponding author at: School of Civil Engineering, Wuhan University, No. 8, East Lake South Road, Wuhan, PR China.
E-mail address: lizhihuang@whu.edu.cn (L.-Z. Huang).

https://doi.org/10.1016/j.jhazmat.2021.126458
Received 12 May 2021; Received in revised form 15 June 2021; Accepted 20 June 2021
Available online 24 June 2021

electroconductivity of groundwater. A suitable electrocatalyst could to greatly reduce the reduction potential of TCE and increase the selectivity for reductive dechlorination, thereby reducing energy consumption and improving the efficiency of groundwater remediation. Therefore, developing efficient, stable, and cheap electrocatalysts is the key to the promotion and application of electrochemical dechlorination in groundwater remediation.

Iron, as the most abundant transition element on earth, is widely used in groundwater remediation involving TCE removal (Cheng and Wu, 2000; Liu et al., 2014). Some modified iron minerals are capable of reducing TCE (Lee and Batchelor, 2003; Y et al., 2007; Liang et al., 2009; Han and Yan, 2016). However, the surface of iron minerals possessing reductive activity are easily passivated (Liu et al., 2005; Yuankui et al., 2016), resulting in the generation of partially dechlorinated products of TCE such as dichloroethylene (DCE) and vinyl chloride (VC) (Little et al., 1988; Ai et al., 2019). These partially dechlorinated products are more challenging to be dechlorinated compared with TCE. Also, they are highly toxic and threaten the ecological systems and human health (Gushgaridoyle and Alvarezcohen, 2020). It should be noted that some anaerobic microorganisms can reduce TCE to DCE and VC (Sharma and Mccarty, 1996). Studies have proved that the active sites for dechlorination in these microorganisms are metal-porphyrin structures, such as coenzyme F430, cobalamin, heme, vitamin B12, etc. (KlecKa and Gonsior, 1984; Krone et al., 1989; Ukrainczyk et al., 1995). Iron-porphyrin is a common iron organic complex in which the four pyrrole rings are connected by methine bridges to form a ring, and an oxidized iron (Fe^{3+}) is located in the center of the ring. Microorganisms transfer electrons to the iron-porphyrin structure to generate a reduced Fe center, which is active for reductive dechlorination. Recently, iron-nitrogen-doped carbon (FeNC) catalysts mimicking iron-porphyrin structure were used to dechlorinate cis-DCE (Gan et al., 2021; Gan et al., 2020). These studies focus on the production of ethylene as a high-value product through dechlorination of cis-DCE in a nonaqueous phase. In contrast, electrochemical detoxification of TCE in groundwater at environmental-related conditions using biomimetic FeNC catalysts has never been studied.

In this work, biomimetic FeNC electrocatalysts were synthesized by pyrolyzing cheap metal salts and nitrogen-containing organic molecules under various temperatures. The as-synthesized FeNC catalysts were characterized and tested for electrochemical dechlorination of TCE in synthetic and real groundwater. All the dechlorination products were analyzed and the stability of the FeNC catalysts was tested. The mechanism of TCE dechlorination was elucidated by DFT calculations and electrochemical analysis.

2. Experimental

2.1. Chemicals

Details on chemical reagents, synthesis of FeNC, fabrication of FeNC working electrode, and computations are provided in Supporting Information. The schematic illustration for FeNC synthesis is shown in Fig. S1. The biomimetic FeNC catalysts were synthesized by pyrolyzing the mixture of *o*-phenylenediamine, silica and $FeCl_3$. FeNC synthesized at 900, 1000 or 1100 °C were designated as FeNC-900, FeNC-1000 or FeNC-1100, respectively.

2.2. FeNC characterization

The crystalline structure of FeNC was analyzed using X-ray diffraction (XRD, X′Pert PRO, PANalytical, Holland). The chemical composition of FeNC was characterized via X-ray photoelectron spectroscopy (XPS, ESCALAB250Xi, Thermo VG Scientific, USA). The structure defect of FeNC was characterized by Raman spectra (Raman, RM1000, Renishaw, UK). The microscopic morphology of FeNC was analyzed by transmission electron microscopy (TEM, JEM-2100, JEOL, Japan).

2.3. Analytical methods

The concentrations of TCE and the dechlorination products (e.g. ethylene and ethane) were measured by a gas chromatograph (GC, GC2010, Shimadzu, Japan) equipped with an electron capture detector (ECD) and a flame ionization detector (FID). The headspace gas with a volume of 200 μL was collected using a gas-tight syringe for the determination. Standard ethylene or ethane gas was injected into the electrochemical cell to draw the standard curve for gas quantification. The temperatures of inlet, column thermostat, ECD and FID were set as 180 °C, 40 °C, 250 °C, and 250 °C, respectively. The concentration of Cl^- was detected via an ion chromatograph (IC, ICS-5000, Thermo Fisher Scientific, USA). Electrochemical analyses, including cyclic voltammetry (CV), electrochemical impedance spectroscopy (EIS), and chronoamperometry (i-t curve), were conducted using an electrochemical workstation (CHI 600E, CH Instruments, USA). The conductivity of a solution was measured by a conductivity meter (DDSJ-318, LEICI, China). Any possible released iron ions during the use of FeNC catalyst were determined by inductive coupled plasma emission spectrometer (ICP-AES, IRIS Intrepid II XSP, USA).

2.4. Experimental setup

The electrochemical removal of TCE was conducted in a glass reactor with a volume of 55 mL (Fig. S2). The reactor contained 50 mL of 2 mM Na_2SO_4 solution simulating groundwater and 5 mL of headspace. The FeNC catalyst was deposited on a glassy carbon plate (2×2 cm) as a working electrode and experiment details are shown in Supporting Information. The counter electrode and reference electrode were Pt plate (2×2 cm) and Ag/AgCl electrode, respectively. All electrode sockets and sampling port were sealed using a tetrafluoroethylene cushion. The parallel distance between the cathode and the anode was 10 mm. TCE saturated water (150 μL) was added into the Na_2SO_4 solution to obtain an initial TCE concentration of 25 μM. The initial pH value was 7.0 and the pH value was adjusted using 0.01 M HCl or 0.01 M NaOH aqueous solutions. The speed of the magnetic stirrer was set to 500 rpm. Reaction solution with a volume of 300 μL was sampled for the determination of TCE and Cl^- concentrations. The FeNC electrode was reused in five consecutive cycles for TCE removal in real groundwater. The FeNC electrode was rinsed and dried between each reuse cycle.

3. Results and discussion

3.1. Characterization of FeNC catalyst

TEM images (Fig. 1a) show that all FeNC materials have nanosheet-like morphology, but the nanosheets morphology of FeNC-1000 and FeNC-1100 were more evident than those of FeNC-900. In addition, high-resolution TEM images of FeNC-1000 and FeNC-1100 show interplanar spacing of 2.16 and 3.47 Å assigned respectively to the 101 and 002 planes of graphene (Fig. S3), but similar layer lattice was not observable in FeNC-900 (Fig. 1b). Importantly, no iron nanoparticles were observed in TEM images. The two XRD diffraction peaks at 25.6° and 43.5° corresponding to the 002 and 101 planes of graphene (Fig. 1c), which is in agreement with the interplanar spacing obtained from the TEM analysis (Gan et al., 2020). The intensity of these two peaks increased with the increase in pyrolysis temperature, demonstrating that higher pyrolysis temperature results in a higher degree of graphitization of the as-synthesized FeNC catalyst (Wang et al., 2018). Notably, no metallic crystalized Fe species was detected by XRD confirming the absence of iron nanoparticles in FeNC catalysts, which is in agreement with the TEM observation. The Raman spectra (Fig. 1d) showed the typical sp^3 defect peak (D band) at 1348 cm^{-1} and the sp^2−bonded carbon (G band) at 1600 cm^{-1}. The I_D/I_G values of FeNC-900 (1.33), FeNC-1000 (1.39), and FeNC-1100 (1.30) were not significantly different, indicating that the degree of disorder in FeNC

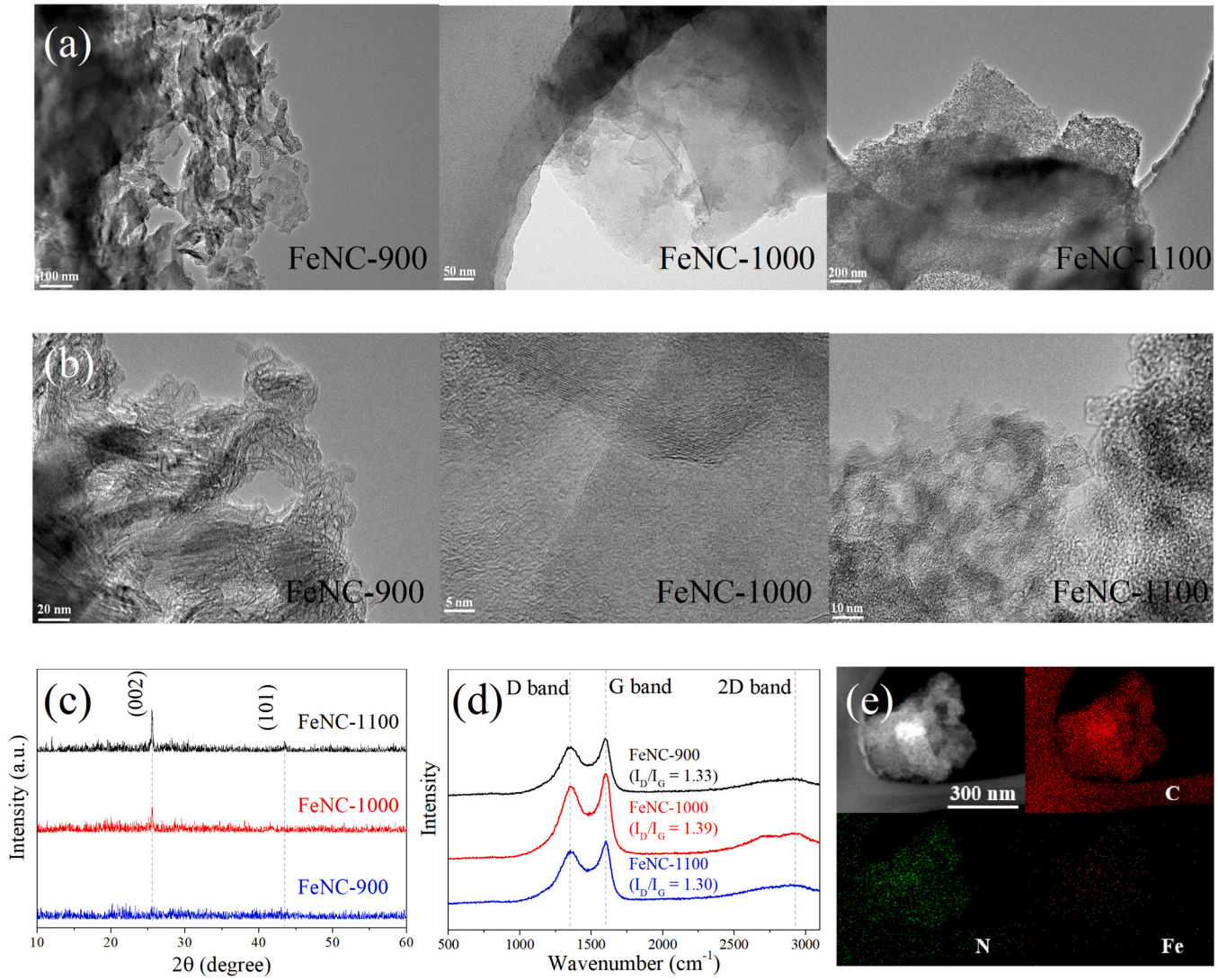

Fig. 1. (a) TEM and (b) High-resolution TEM images, (c) XRD patterns, (d) Raman spectra of FeNC-900, FeNC-1000, and FeNC-1100, and (e) elemental mapping of FeNC-1000.

materials was similar (Jing et al., 2018). The energy-dispersive X-ray spectroscopy (EDS) elemental mapping confirmed that Fe and N are evenly distributed over the entire carbon nanosheets of FeNC-1000 catalysts (Fig. 1e). Therefore, it is reasonable to claim that the Fe is atomically dispersed in FeNC.

The active site of biomimetic FeNC material is expected to be the iron-porphyrin structure. Thus, the species of N and Fe were identified via XPS analysis. Four peaks at 398.1, 399.0, 400.5, and 403.0 eV were pyridinic N, pyrrolic N, graphitic N and oxidized N, respectively (Fig. 2a) (Gan et al., 2020). The relative content of different N species is shown in Fig. 2b and Table S1. With synthesis temperature increasing, the relative content of graphitic N increased and the content of pyridinic N decreased. It conforms to the high degree of graphitization at high synthesis temperature, which is also confirmed by XRD analysis. The Fe 2p spectra in Fig. 2c showed peaks at 710.8 and 723.2 eV belonging to Fe^{2+} and peaks at 714.6 and 726.8 eV attributed to Fe^{3+} (Xiao et al., 2019). Based on the survey spectra (Fig. 2d), the contents of Fe in FeNC-900, FeNC-1000, and FeNC-1100 were determined to be 0.87, 0.21, and <0.10 atom %, respectively. This gave an indication that the Fe contents in FeNC catalysts decreased significantly with the increase in synthesis temperature. For the iron-porphyrin like structure of FeNC, pyridinic N is the site for fixing Fe atoms through coordination (Ma et al., 2018). The high pyrolysis temperature resulted in the decrease of pyridinic N content, thereby reducing the content of coordinated Fe atoms (Fe-N_4) in FeNC.

3.2. Electrochemical reduction of TCE by FeNC catalysts

The biomimetic FeNC was deposited on the surface of a glassy carbon electrode and the electrocatalytic performance of FeNC for TCE removal was evaluated in synthetic groundwater with a low electrolyte concentration (2 mM Na_2SO_4). FeNC-900, FeNC-1000, and FeNC-1100 showed almost the same adsorption efficiency of ~35% towards TCE at open circuit potential (Fig. S5). The FeNC has a large surface area and porosity which is beneficial for TCE adsorption (Jingchun et al., 2016). Meanwhile, there were no reduction products detected, indicating that FeNC materials cannot dechlorinate TCE without applying a potential. Thus, the different catalytic performances of FeNCs in TCE removal are mainly attributed to their intrinsic catalytic activity.

The bare glassy carbon electrode showed only 22.5%, 34.0% and 32.5% of TCE removal at −0.8 V, −1.0 V and −1.2 V, respectively (Fig. 3a–c). However, the production of completely dechlorinated products from TCE reduction is much negative than −1.2 V (Lei et al., 2019). Thus, TCE may be transformed into toxic partially dechlorinated products by bare glassy carbon electrode. In contrast, FeNC electrocatalytic cathode showed excellent TCE removal efficiency. TCE

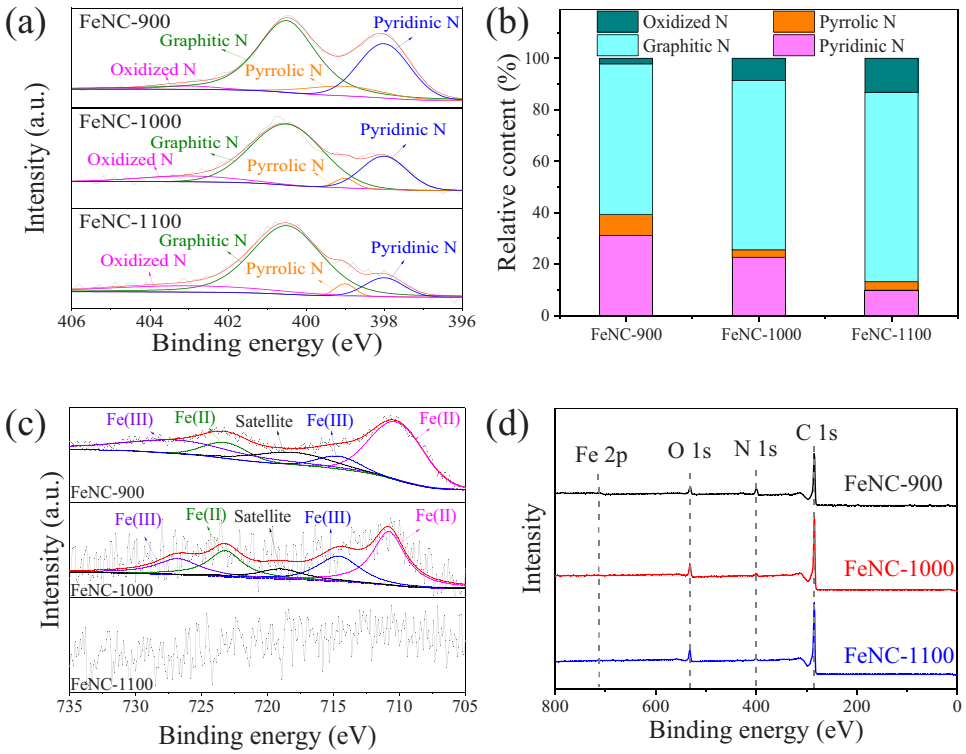

Fig. 2. (a) N 1s XPS, (b) the relative content of N species, (c) Fe 2p XPS; (d) XPS survey spectra of FeNC-900, FeNC-1000 and FeNC-1100.

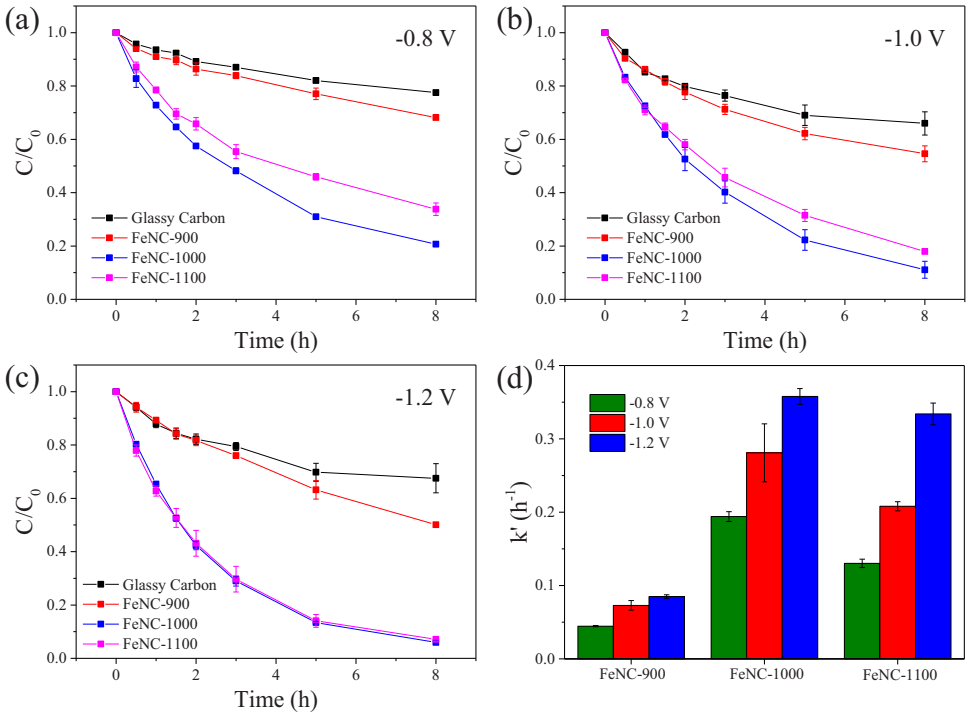

Fig. 3. Electrochemical reduction of TCE using FeNC catalysts at (a) −0.8 V, (b) −1.0 V and (c) −1.2 V vs. Ag/AgCl. (d) Pseudo first-order reaction rate constants of TCE degradation under different potentials. Reaction condition: 2 mM Na_2SO_4 electrolyte, pH=7.0, initial TCE concentration=25 μM.

removal efficiency is over 80% with FeNC-1000 and FeNC-1100 cathode at −1.0 V and −1.2 V. Through the pseudo-first-order reaction kinetic fitting, rate constants of TCE removal (k′) increased at a more negative potential (Fig. 3d, Fig. S4). Comparing with FeNC-900 and FeNC-1100, FeNC-1000 had the highest k′ value which were 0.19, 0.28 and 0.36 h^{-1} at −0.8 V, −1.0 V and −1.2 V, respectively. The stable current density during the electrolysis at −1.0 V indicated the high stability of FeNC cathodes towards TCE reduction (Fig. S6). The current density of FeNC-1100 was larger than that of FeNC-1000, although FeNC-1100 had a lower catalytic performance for TCE removal. The results demonstrate

that the current efficiency for TCE reduction by FeNC-1000 was much higher than FeNC-1100 under the same experimental conditions.

3.3. Effect of dissolved oxygen

To explore the effect of dissolved oxygen on TCE removal, Na_2SO_4 electrolyte was bubbled with argon or dioxygen before the TCE reduction experiment. The removal rate of TCE was decreased from 0.29 to 0.21 h^{-1} in an O_2-saturated electrolyte (Fig. 4). The absence of O_2 in electrolyte slightly increased the initial rate from 0.29 to 0.30 h^{-1}. Although dissolved oxygen could compete with TCE for the reductive sites, FeNC-1000 still maintains a high removal efficiency of TCE. These results indicate the high selectivity of FeNC-1000 catalyst towards TCE reduction under ambient conditions.

3.4. Effect of pH

No lesser-chlorinated by-products were detected during electrolysis. In contrast, ethylene (C_2H_4) and ethane (C_2H_6), as the complete dechlorination products of TCE, were detected in the FeNC electrochemical system. After 8-hour electrolysis, the production of C_2H_4 and C_2H_6 were 2.4% and 70.6% at pH 5.0 (Fig. 5a). At pH 7.0, the yields of C_2H_4 and C_2H_6 were 6.5% and 25.6%, respectively (Fig. 5b). At pH 9.0, the production yields of C_2H_4 and C_2H_6 were 13.3% and 13.2%, respectively (Fig. 5c). TCE removal efficiency was close under different pH conditions (Fig. 5d), indicating that the influence of pH value on TCE removal was negligible. However, the production of C_2H_4 increased slightly and the production of C_2H_6 decreased significantly with pH value increasing. The generation of C_2H_6 involves the hydrogenation reaction of C_2H_4. The proton H^+ obtain electron on the surface of FeNC electrode to form active hydrogen (H*) which attacks the unsaturated C=C bond in C_2H_4 to form C_2H_6. Thus, the yield of C_2H_6 was highest in acidic condition comparing with neutral and alkaline conditions. Although the TCE removal efficiency was similar at different pHs, acidic condition accelerates the transformation from TCE to C_2H_6 on the surface of FeNC-1000. The whole process of TCE dechlorination includes two steps. The first step is the diffusion of TCE in the bulk solution to the surface of FeNC, which is represented by the removal efficiency of TCE. The second step is the transformation of TCE on the surface of FeNC, which is characterized by the production of complete dechlorination products. The role of H* may be more obvious in the second step.

3.5. The role of H*

The presence of C_2H_6 may be resulted from the H*-involving dechlorination of TCE. Therefore, Tert-butyl alcohol (TBA) as a H* quencher was introduced into the electrolyte in this work (Zhang et al., 2019). The inhibitory effect of TBA on TCE removal was relatively close in the presence of TBA with varying concentrations from 50 to 200 mM (Fig. 6a). The distribution of dechlorination products during electrolysis in the presence of 100 mM TBA was shown in Fig. S7. TCE removal efficiency and the yield of complete dechlorination products decreased ~10% in the presence of 100 mM TBA (Fig. 6b). The high concentration of TBA cannot efficiently suppress the TCE removal demonstrating that the generated H* is more likely adsorbed on the surface of FeNC rather than in bulk solution. The diffusion of TBA onto the FeNC surface may be the rate-limiting step for the H* quenching by TBA.

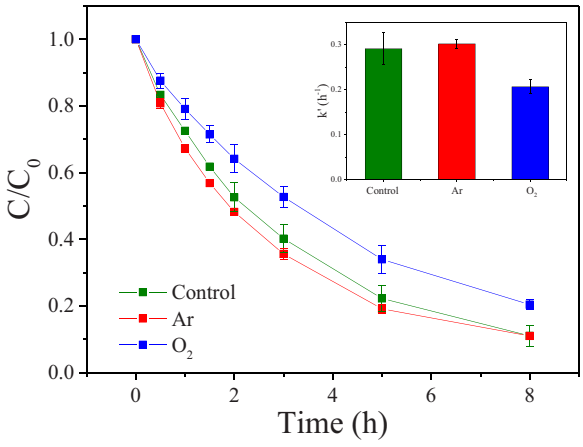

Fig. 4. TCE removal by FeNC-1000 cathode in Ar and O_2-saturated solutions. Reaction conditions: applied potential=−1.0 V; electrolyte=2 mM Na_2SO_4; pH=7.0; initial TCE concentration=25 μM.

3.6. Mechanism

Reaction was carried out in a divided electrochemical reactor to investigate the effect of Pt anode on TCE degradation (Fig. S8). TCE removal was negligible and no degradation products (e.g. partially dechlorinated compounds, C_2H_4, and C_2H_6) were observed in the anodic chamber (Fig. S9), demonstrating that Pt anode did not contribute to the degradation of TCE.

Electrochemical impedance spectroscopy (EIS) analysis was conducted to investigate the properties of electron transfer for FeNC. The smallest arc radius for FeNC-1000 in EIS demonstrated the fastest interfacial electron transfer rate on the surface of FeNC-1000 comparing with FeNC-900 and FeNC-1100 (Fig. 7a) (Zhang et al., 2019). The TCE reduction current derived for FeNC-1000 is the largest among all the FeNC catalysts (Fig. 7b), demonstrating the highest electron transfer rate from FeNC-1000 cathode to TCE. Liu and coworkers reported a novel graphene-like biochar calcined at an elevated temperature with an excellent electron transfer rate; such evidence may explain our observation of a higher TCE reduction by the FeNC-1000 (Liu et al., 2021). Therefore, the highest reduction rate of TCE was observed using the FeNC-1000 catalyst. To determine the electrochemically active surface area of FeNC, the non-faradaic capacitive current densities were calculated via cyclic voltammograms of FeNCs with different scan rates (Fig. S10) (Benck et al., 2012). The current density increase with the scan rates (Fig. 7c), which conform to capacitive charging behavior (Miao et al., 2015). The greater slope of the curve for FeNC-1000 demonstrates that FeNC-1000 has a higher total electrochemically active surface area compared with FeNC-900 and FeNC-1100 (Xin-Ming et al., 2018). A higher total electrochemically active surface area of FeNC-1000 results in a higher electron transfer efficiency, resulting in a higher TCE removal rate. The high pyrolysis temperature at 1100 °C reduced the content of pyridinic N and the Fe–N active sites of FeCN-1100 as demonstrated by the low Fe content in FeCN-1100 (Fig. 2b). FeNC-900 has the highest Fe content and highest pyridinic N content but the lowest TCE removal efficiency among the FeNC catalysts. Thus, the removal and transformation of TCE may involve the synergy between different forms of N and Fe–N active sites.

The mechanism of TCE dechlorination was further reveal by density functional theory (DFT) analysis. Various adsorption sites for TCE on FeNC surface, including graphene, graphitic N doped graphene, pyrrolic N doped graphene, pyridinic N doped graphene and Fe-N_4 structure of FeNC, were optimized via DFT (Fig. S11). Adsorption and subsequent electron transfer play essential roles during TCE reduction on the surface of catalysts (Gan et al., 2020). The adsorption energies of TCE on the different adsorption sites were calculated (Fig. 8a–e, Table S2). These adsorption energy values were close to zero suggesting that the TCE molecules can easily have physical contact with the surface of FeNC. The electron transfer between FeNC and TCE molecule was examined in Fig. 8f. When TCE approaches Fe atoms, electrons (sky blue) mainly locate on all the three C−Cl bonds. Thus, complete reductive dechlorination with breakage of all the three C−Cl bonds can be easily obtained once electrons are transferred directly or indirectly via H* from FeNC to TCE molecules. As a result, the partially dechlorinated intermediates

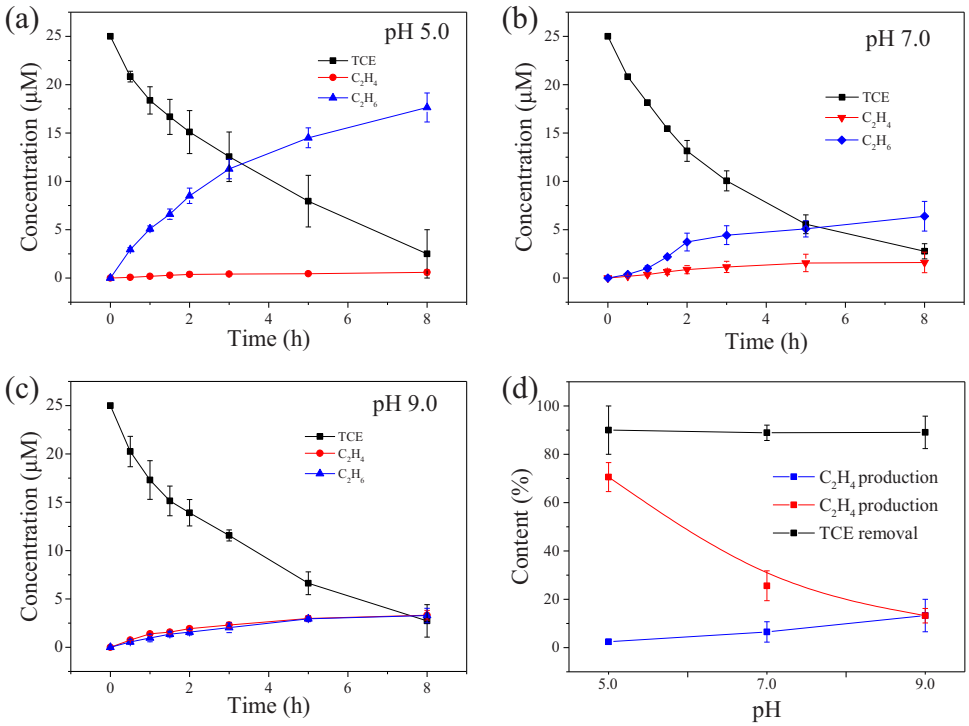

Fig. 5. Dechlorination products of TCE using FeNC-1000 cathode at (a) pH 5.0, (b) pH 7.0 and (c) pH 9.0. (d) TCE removal and ethane and ethylene production efficiency after 8 h reaction under different pHs. Reaction condition: 2 mM Na_2SO_4 electrolyte, applied potential=−1.0 V, initial TCE concentration=25 μM.

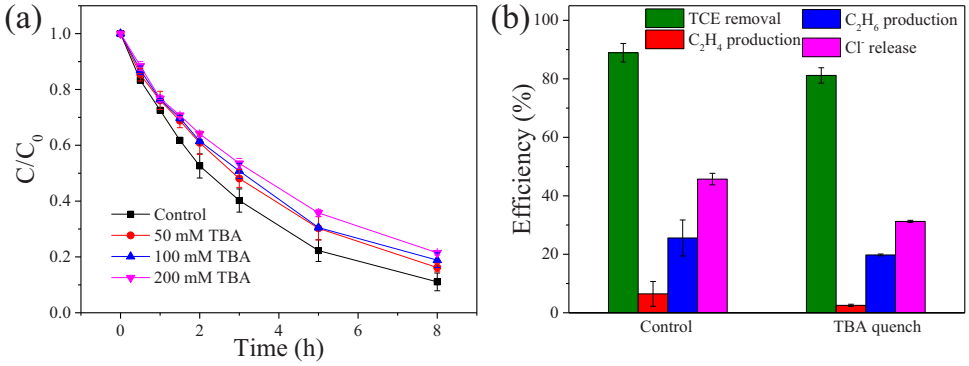

Fig. 6. (a) Effect of TBA on TCE removal. (b) Dechlorination products of TCE with the presence of 100 mM TBA. Reaction condition: FeNC-1000 cathode, 2 mM Na_2SO_4 electrolyte, applied potential=−1.0 V, pH=7.0, initial TCE concentration=25 μM.

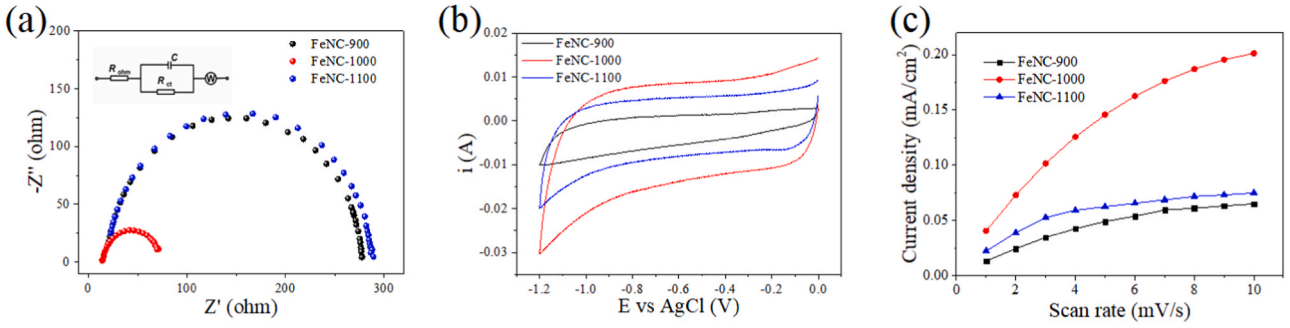

Fig. 7. (a) Electrochemical impedance spectra of FeNCs. Inset: equivalent circuit used for data analysis, (b) cyclic voltammograms of FeNCs, and (c) plots of capacitive currents vs. scan rates of FeNC electrodes.

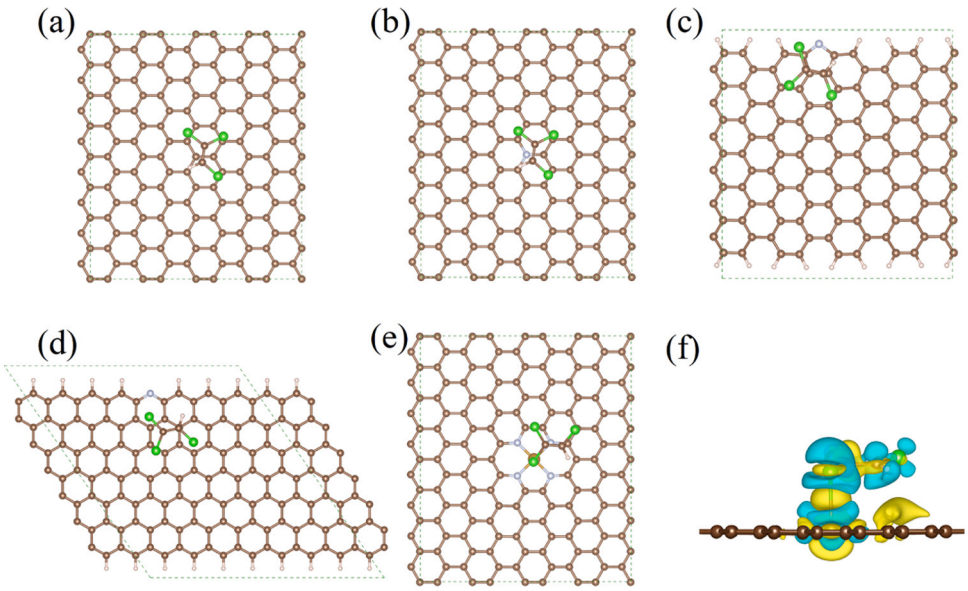

Fig. 8. Optimized configuration of (a) graphene, (b) graphitic N doped graphene, (c) pyrrolic N doped graphene, (d) pyridinic N doped graphene, and (e) Fe-N_4 structure of FeNC with TCE. (f) Charge density difference for optimized configurations of TCE adsorbed on FeNC. The blue and yellow denote the electron accumulation and electron depletion, respectively, the isosurface of charge density was set to 0.0002 e $Å^{-3}$. (For interpretation of the references to color in this figure legend, the reader is referred to the web version of this article).

were not observed in this work (Fig. S12). In addition, the conformations of various partially dechlorinated intermediates, including cis-DCE, trans-DCE, 1,1-DCE and vinyl chloride (VC), on FeNC surface was optimized (Fig. S13). The very close adsorption energy values of these conformations demonstrate that the FeNC surface does not strongly adsorb these partially dechlorinated intermediates (Table S3). Thus, the absence of toxic partially dechlorinated intermediates in the reaction solution is attributed to the fast dechlorination of TCE to fully dechlorinated products rather than the increased adsorption of partially dechlorinated intermediates on the FeNC surface. Studies show that graphitic N in graphene enhances the electrochemical hydrogen evolution reaction (HER) (Lin et al., 2019). Thus, the generation of H* as an intermediate in HER may be favored in the presence of graphitic N in FeNC catalyst. As a result, H* react with TCE to form non-toxic fully dechlorinated products such as C_2H_4 and C_2H_6.

The mechanism of TCE reduction by FeNC cathode was proposed in Fig. 9. Firstly, the TCE molecule was adsorbed on the surface of FeNC. FeNC-900, FeNC-1000 and FeNC-1100 had similar TCE adsorption effects at open circuit potentials. However, once potentials were applied, the FeNCs showed different TCE efficiencies due to the different atomic structure of FeNC. Pyridinic N coordinate Fe atoms, forming Fe-N_4 active sites for electron transfer from FeNC to TCE. Graphitic N generated H* to attack C–Cl bonds of TCE. TCE was reduced to complete dechlorination products followed by the desorption from the FeNC surface. Subsequently, the active sites of FeNC are regenerated after the desorption process. The optimal content of graphitic N and pyridinic N in FeNC-1000 resulted in the most efficient TCE dechlorination process comparing with FeNC-900 and FeNC-1100.

3.7. Application to groundwater remediation

Real groundwater was used to evaluate the possible practical application of the biomimetic FeNC catalyst. TCE removal rate in real groundwater was similar to that in Na_2SO_4 electrolyte, which demonstrating FeNC is a promising electrocatalyst for groundwater remediation. The resistivity of the real groundwater and synthetic groundwater (2 mM Na_2SO_4) was 1.765±0.015 kΩ cm and 2.445±0.005 kΩ cm, respectively. The similar solution conductivity may lead to the similar TCE removal efficiency in both real and synthetic groundwater. The conductivity of real groundwater is due to the presence of various anions (Table S4). In order to test the reusability and stability of FeNC cathode, the catalyst was recycled and reused five times in real groundwater (Fig. 10b). TCE removal efficiencies were above 95% and the current densities were higher than 0.5 mA cm^{-2} for the five cycles. Only a slight decrease in efficiency was observed which can be due to the superiority of the Fe-N sites resisting to the background ions (e.g. phosphate) compared to that of iron oxides (Fang et al., 2018). The C_2H_4 production yields for the five cycles were 10.3%, 11.2%, 10.2%, 11.0% and 11.4%, respectively. The C_2H_6 production yields were 35.9%, 36.4%, 33.7%, 34.2% and 35.6%, respectively. For each cycle, the reduction products are non-toxic permanent gas without any formation of toxic partially dechlorinated intermediates. The dissolved iron ions were not detected in the cycle experiment, which can be attributed to the low iron content in FeNC (0.21%) and the stabilized iron atoms in FeNC via Fe-N bonding.

This work is the proof of concept that biomimetic FeNC is promising for the practical remediation of TCE contaminated groundwater. It should be noted that no toxic partially dechlorinated products were formed during the whole TCE dechlorination process, which is important for practical applications. Usually, noble metal-based catalyst is needed to avoid the formation of toxic lesser-chlorinated intermediates during remediation of HOPs-contaminated groundwater (Liu et al., 2018). Simultaneous removal of HOPs and heavy metals using the FeNC catalyst is also expected (Liu et al., 2020; Fang et al., 2020). However, several challenges, such as catalysts shedding, limitations of underground space etc., may need to be overcome for the real application of this process and further testing is needed in bench scale and pilot scale.

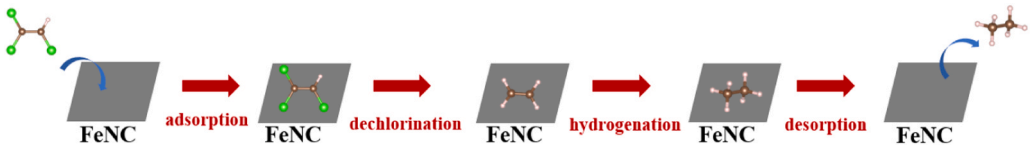

Fig. 9. Schematic diagram of TCE reduction mechanism.

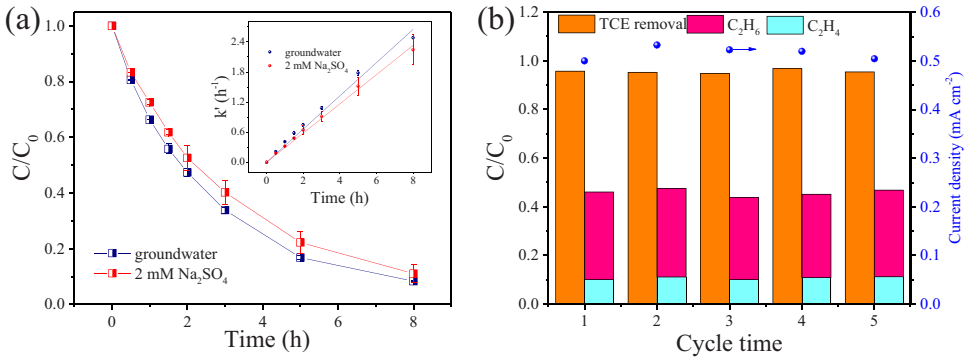

Fig. 10. (a) TCE reduction in 2 mM Na_2SO_4 aqueous solution and in real groundwater; (b) experiments testing reuse performance of FeNC. The data points in blue color represent the current density during the cycle experiments. Reaction conditions: potential=−1.0 V; pH=7.0; TCE initial concentration=25 μM. (For interpretation of the references to color in this figure legend, the reader is referred to the web version of this article).

4. Conclusion

This study presented results on the synthesis, characterization, and performance evaluation of biomimetic FeNC loaded on the surface of glassy carbon cathode for the electrochemical dechlorination of TCE. Results on the synthesis of FeNC catalysts via pyrolysis at 900, 1000, and 1100 °C and their characterization show that higher pyrolysis temperature results in a higher degree of graphitization of the as-synthesized FeNC. FeNC-1000 had the largest electrochemical active surface area and the highest electron transfer efficiency leading to the best TCE removal efficiency among FeNC catalysts. DFT calculations suggests that electrons are transferred from Fe-N_4 active sites to TCE molecules for TCE dechlorination, and H^+ is activated by graphitic N to form H* causing the transformation of TCE to C_2H_6. In studies using real groundwater as a solution matrix, FeNC-1000 showed excellent TCE removal efficiency. No toxic intermediate products were observed during the reuse of the FeNC catalyst. In summary, electrochemical reductive remediation of TCE contaminated groundwater using biomimetic FeNC catalyst was feasible, but more studies are needed in bench scale experiments and pilot scale demonstrations before full assessment of this technology is made.

CRediT authorship contribution statement

Jia Deng: Validation, Investigation, Writing - original draft. **Xin-Ming Hu:** Writing - review & editing. **Enlai Gao:** Formal analysis. **Feng Wu:** Supervision, Funding acquisition. **Weizhao Yin:** Supervision, Funding acquisition. **Li-Zhi Huang:** Conceptualization, Methodology, Project administration, Funding acquisition, Investigation. **Dionysios D. Dionysiou:** Writing - review & editing.

Declaration of Competing Interest

The authors declare that they have no known competing financial interests or personal relationships that could have appeared to influence the work reported in this paper.

Acknowledgements

The current work was financially supported by the National Natural Science Foundation of China (Grant No. 41807188 and 51978537) and the Fundamental Research Funds for the Central Universities (2042021kf0201). D.D. Dionysiou acknowledges support from the University of Cincinnati through the Herman Schneider Professorship in the College of Engineering and Applied Sciences.

Appendix A. Supporting information

Supplementary data associated with this article can be found in the online version at doi:10.1016/j.jhazmat.2021.126458.

References

Ai, J., Yin, W., Hansen, H.C.B., 2019. Fast dechlorination of chlorinated ethylenes by green rust in the presence of bone char. Environ. Sci. Technol. Lett. 6, 191–196.
Antonello, S., Maran, F., 1999. The role and relevance of the transfer coefficient α in the study of dissociative electron transfers: concepts and examples from the electroreduction of perbenzoates. J. Am. Chem. Soc. 121, 9668–9676.
Benck, J.D., Chen, Z., Kuritzky, L.Y., Forman, A.J., Jaramillo, T.F., 2012. Amorphous molybdenum sulfide catalysts for electrochemical hydrogen production: insights into the origin of their catalytic activity. ACS Catal. 2, 1916–1923.
Cheng, S.F., Wu, S.C., 2000. The enhancement methods for the degradation of TCE by zero-valent metals. Chemosphere 41, 1263–1270.
Durante, C., Isse, A.A., Gennaro, A., 2013. Electrocatalytic dechlorination of polychloroethylenes at silver cathode. J. Appl. Electrochem. 43, 227–235.
Fang, L., Liu, R., Li, J., Xu, C., Huang, L.-Z., Wang, D., 2018. Magnetite/Lanthanum hydroxide for phosphate sequestration and recovery from lake and the attenuation effects of sediment particles. Water Res. 130, 243–254.
Fang, L., Liu, K., Li, F., Zeng, W., Ma, Y., 2021. New insights into stoichiometric efficiency and synergistic mechanism of persulfate activation by zero-valent bimetal (Iron/Copper) for organic pollutant degradation. J. Hazard. Mater. 403, 123669.
Gan, G., Li, X., Fan, S., Yin, Z., Wang, L., Chen, G., 2021. Ultrathin Fe–N –C single-atom catalysts with bifunctional active site for simultaneous production of ethylene and aromatic chlorides. Nano Energy 80, 105532.
Gan, G., Li, X., Wang, L., Fan, S., Mu, J., Wang, P., Chen, G., 2020. Active sites in single-atom Fe-N_x-C nanosheets for selective electrochemical dechlorination of 1,2-dichloroethane to ethylene. ACS Nano 14, 9929–9937.
Gushgaridoyle, S., Alvarezcohen, L., 2020. Effects of arsenic on trichloroethene–dechlorination activities of dehalococcoides mccartyi 195. Environ. Sci. Technol. 54, 1276–1285.
Han, Y., Yan, W., 2016. Reductive dechlorination of trichloroethene by zero-valent iron nanoparticles: reactivity enhancement through sulfidation treatment. Environ. Sci. Technol. 50, 12992–13001.
He, B., He, J., Wang, L., Zhang, X., Bi, E., 2019. Effect of hydrogeological conditions and surface loads on shallow groundwater nitrate pollution in the Shaying river basin: based on least squares surface fitting model. Water Res. 163, 114880.
Van Hoomissen, D.J., Vyas, S., 2019. Early events in the reductive dehalogenation of linear perfluoroalkyl substances. Environ. Sci. Technol. Lett. 6, 365–371.
Huang, L.Z., Hansen, H.C.B., Bjerrum, M.J., 2015. Electrochemical reduction of nitroaromatic compounds by single sheet iron oxide coated electrodes. J. Hazard. Mater. 306, 175–183.
Jingchun, Y., Weiguo, G., Mingang, D., Lu, H., Linbo, Q., 2016. Degradation of trichloroethylene by activated persulfate using a reduced graphene oxide supported magnetite nanoparticle. Chem. Eng. J. 295, 309–316.
Jing, B., Baojuan, X., Hongzhi, M., Yue, L., Xiaojian, M., Jinkui, F., Shenglin, X., 2018. One-step construction of N,P-codoped porous carbon sheets/CoP hybrids with enhanced lithium and potassium storage. Adv. Mater. 30, 1802310.
KlecKa, G.M., Gonsior, S.J., 1984. Reductive dechlorination of chlorinated methanes and ethanes by reduced iron (II) porphyrins. Chemosphere 13, 391–402.
Krone, U.E., Laufer, K., Thauer, R.K., Hogenkamp, H.P.C., 1989. Coenzyme F430 as a possible catalyst for the reductive dehalogenation of chlorinated C1 hydrocarbons in methanogenic bacteria. Biochemistry 28, 10061–10065.
Lee, W., Batchelor, B., 2003. Abiotic reductive dechlorination of chlorinated ethylenes by iron bearing soil minerals. 1. pyrite and magnetite. Environ. Sci. Technol. 36, 5147–5154.
Lei, C., Liang, F., Li, J., Chen, W., Huang, B., 2019. Electrochemical reductive dechlorination of chlorinated volatile organic compounds (Cl-VOCs): effects of

molecular structure on the dehalogenation reactivity and mechanisms. Chem. Eng. J. 358, 1054–1064.
Liang, X., Philp, R.P., Butler, E.C., 2009. Kinetic and isotope analyses of tetrachloroethylene and trichloroethylene degradation by model Fe(II)-bearing minerals. Chemosphere 75, 63–69.
Lin, Z., Yang, Y., Li, M., Huang, H., Chen, Q.W., 2019. Dual graphitic-N doping in a six-membered C-ring of graphene-analogous particles enables an efficient electrocatalyst for the hydrogen evolution reaction. Angew. Chem. Int. Ed. 58, 16973–16980.
Little, C.D., Palumbo, A.V., Herbes, S.E., Lidstrom, M.E., Tyndall, R.L., Gilmer, P.J., 1988. Trichloroethylene biodegradation by a methane-oxidizing bacterium. Appl. Environ. Microb. 54, 951–956.
Liu, H., Bruton, T.A., Doyle, F.M., Sedlak, D.L., 2014. In situ chemical oxidation of contaminated groundwater by persulfate: decomposition by Fe(III)- and Mn(IV)-containing oxides and aquifer materials. Environ. Sci. Technol. 48, 10330–10336.
Liu, R., Chen, H.-m, Fang, L.-p, Xu, C., He, Z., Lai, Y., 2018. Au@Pd bimetallic nanocatalyst for carbon-halogen bond cleavage: an old story with new iInsight into how the activity of pd is influenced by Au. Environ. Sci. Technol. 52, 4244–4255.
Liu, K., Li, F., Cui, J., Yang, S., Fang, L., 2020. Simultaneous removal of Cd(II) and As(III) by graphene-like biochar-supported zero-valent iron from irrigation waters under aerobic conditions: Synergistic effects and mechanisms. J. Hazard. Mater. 395, 122623.
Liu, K., Li, F., Zhao, X., Wang, G., Fang, L., 2021. The overlooked role of carbonaceous supports in enhancing arsenite oxidation and removal by nZVI: surface area versus electrochemical property. Chem. Eng. J. 406, 126851.
Liu, Y., Majetich, S.A., Tilton, R.D., Sholl, D.S., Lowry, G.V., 2005. TCE dechlorination rates, pathways, and efficiency of nanoscale iron particles with different properties. Environ. Sci. Technol. 39, 1338–1345.
Li, K., Stefan, M.I., Crittenden, J.C., 2004. UV photolysis of trichloroethylene: product study and kinetic modeling. Environ. Sci. Technol. 38, 6685–6693.
Mao, R., Huang, C., Zhao, X., Ma, M., Qu, J., 2019. Dechlorination of triclosan by enhanced atomic hydrogen-mediated electrochemical reduction: kinetics, mechanism, and toxicity assessment. Appl. Catal. B 241, 120–129.
Ma, J., Xu, L., Shen, C., Hu, C., Liu, W., Wen, Y., 2018. Fe-N-graphene wrapped Al_2O_3/pentlandite from microalgae: high fenton catalytic efficiency from enhanced Fe^{3+} reduction. Environ. Sci. Technol. 52, 3608–3614.
Miao, L., Feng, C., Hu, W., Zhang, Z., Sugiura, N., 2009. Electrochemical degradation of phenol using electrodes of Ti/RuO_2-Pt and Ti/IrO_2-Pt. J. Hazard. Mater. 162, 455–462.
Miao, J., Xiao, F.-X., Yang, H.B., Khoo, S.Y., Chen, j, Fan, Z., Hsu, Y.-Y., Chen, Hm, Zhang, H., Liu, B., 2015. Hierarchical Ni-Mo-S nanosheets on carbon fiber cloth: a flexible electrode for efficient hydrogen generation in neutral electrolyte. In: Sci. Adv., 1.
Moran, M.J., Zogorski, J.S., Squillace, P.J., 2007. Chlorinated solvents in groundwater of the United States. Environ. Sci. Technol. 41, 74–81.
Murakami, M., Kuroda, K., Sato, N., Fukushi, T., Takizawa, S., Takada, H., 2009. Groundwater pollution by perfluorinated surfactants in Tokyo. Environ. Sci. Technol. 43, 3480–3486.
Prasad, R.K., Srivastava, S.N., 2009. Electrochemical degradation of distillery spent wash using catalytic anode: factorial design of experiments. Chem. Eng. J. 146, 22–29.
Press, D.J., Mckinley, M., Deapen, D., Clarke, C.A., Gomez, S.L., 2016. Residential cancer cluster investigation nearby a superfund study area with trichloroethylene contamination. Cancer Causes Control 27, 607–613.
Schaefer, C.E., Choyke, S., Ferguson, P.L., Andaya, C., Burant, A., Maizel, A., Strathmann, T.J., Higgins, C.P., 2018. Electrochemical transformations of perfluoroalkyl acid (PFAA) precursors and PFAAs in groundwater impacted with aqueous film forming foams. Environ. Sci. Technol. 52, 10689–10697.
Sharma, P.K., Mccarty, P.L., 1996. Isolation and characterization of a facultatively aerobic bacterium that reductively dehalogenates tetrachloroethene to cis-1,2-dichloroethene. Appl. Environ. Microb. 62, 761–765.
Smith, J.A., Tisdale, A.K., Cho, H.J., 1996. Quantification of natural vapor fluxes of trichloroethene in the unsaturated zone at Picatinny arsenal, New Jersey. Environ. Sci. Technol. 30, 2243–2250.
Ukrainczyk, L., Chibwe, M., Pinnavaia, T.J., Boyd, S.A., 1995. Reductive dechlorination of carbon tetrachloride in water catalyzed by mineral-supported biomimetic cobalt macrocycles. Environ. Sci. Technol. 29, 439–445.
Wang, J., Xu, Y., Ding, B., Chang, Z., Zhang, X., 2018. Confined self-assembly in two-dimensional interlayer space: monolayered mesoporous carbon nanosheets with in-plane orderly arranged mesopores and a highly graphitized framework. Angew. Chem. Int. Ed. 57, 2894–2898.
Westrick, J.J., Mello, J.W.N., Thomas, R.F., 1984. The groundwater supply survey. J. Am. Water Works Assoc. 76, 52–59.
Xiao, F., Xu, G.L., Sun, C.J., Xu, M., Wen, W., Wang, Q., Gu, M., Zhu, S., Li, Y., Wei, Z., 2019. Nitrogen-coordinated single iron atom catalysts derived from metal organic frameworks for oxygen reduction reaction. Nano Energy 61, 60–68.
Xin-Ming, H., Halvor HøEn, H., Tveden, B.E., Junker, D.K., Rohde, M.M., Marga-Martina, P., Edmund, W., Paolo, L., Birk, B.K., Martin, B., 2018. Selective CO_2 Reduction to CO in water using earth-abundant metal and nitrogen-doped carbon electrocatalysts. ACS Catal. 8, 6255–6264.
Y, J.H., Kim, H., F, H.K., 2007. Reductive dechlorination pathways of tetrachioroethylene and trichloroethylene and subsequent transformation of their dechlorination products by mackinawite (FeS) in the presence of metals. Environ. Sci. Technol. 41, 7736–7743.
Yin, H., Cao, X., Lei, C., Chen, W., Huang, B., 2020. Insights into electroreductive dehalogenation mechanisms of chlorinated environmental pollutants. Chemelectrochem 7, 1825–1837.
Yuankui, S., Jinxiang, L., Tinglin, H., Xiaohong, G., 2016. The influences of iron characteristics, operating conditions and solution chemistry on contaminants removal by zero-valent iron: a review. Water Res. 100, 277–295.
Zhang, J., Ji, Q., Lan, H., Zhang, G., Liu, H., Qu, J., 2019. Synchronous reduction–oxidation process for efficient removal of trichloroacetic acid: H* initiates dechlorination and·OH is responsible for removal efficiency. Environ. Sci. Technol. 53, 14586–14594.

Supplementary Information for

Electrochemical reductive remediation of trichloroethylene contaminated groundwater using biomimetic iron-nitrogen-doped carbon

Jia Deng[a], Xin-Ming Hu[b], Enlai Gao[a], Feng Wu[c], Weizhao Yin[d], Li-Zhi Huang[a,e]*, Dionysios D. Dionysiou[f]

[a] *School of Civil Engineering, Wuhan University, No. 8, East Lake South Road, Wuhan, P.R. China*

[b] *Environment Research Institute, Shandong University, Qingdao 266237, P.R. China*

[c] *School of Resources and Environmental Science, Wuhan University, Wuhan, P.R. China*

[d] *School of Environment, Jinan University, Guangzhou 510632, P.R. China*

[e] *State Key Laboratory of Water Resources and Hydropower Engineering Science, Wuhan University, 430072, China*

[f] *Environmental Engineering and Science Program, Department of Chemical and Environmental Engineering, University of Cincinnati, Cincinnati, Ohio 45221-0012, United States*

Chemical reagents

TCE, tertiary butyl alcohol (TBA), isopropanol, hydrochloric acid (HCl), sodium hydroxide (NaOH), and sodium sulphate (Na_2SO_4) were purchased from Sinopharm Chemical Reagent Co., Ltd. (Shanghai, China). Iron meso−tetraphenylporphyrin chloride (FeTPP), *o*−phenylenediamine, and colloidal silica suspension were obtained from Sigma−Aldrich (Shanghai, China). All chemical reagents were analytical reagents and aqueous solutions were prepared using ultrapure water (18.2

MΩ.cm). The standard gases including ethane, ethylene, and acetylene were provided by Zhongxinruiyuan Gas Co., Ltd. (Wuhan, China).

Synthesis of FeNC

The synthesis method of FeNC was as reported in our previous work [1]. Briefly, 27.8 mmol of *o*-phenylenediamine was dissolved in 60 mL 1 M HCl followed by addition of Ludox HS40 colloidal silica suspension (Ø ≈ 12 nm, 40 wt. %, 22.5 g) and 13.9 mmol $FeCl_3$. After the mixture was stirred for 15 min, it was concentrated on a rotovap and dried under vacuum. The powder obtained was ground and subjected to pyrolysis at 900, 1000 or 1100 °C for 1 h under an inert Ar atmosphere. The silica template in the material was etched away with 2 M NaOH for 2 days. Subsequently, the iron particles in the material were removed in 0.5 M H_2SO_4 at 90 °C for 4 h. A second pyrolysis was applied under the same conditions as for the first one to give the FeNC material. The illustration of FeNC nanosheets synthesis is shown in Figure S1.

Fabrication of FeNC working electrode

50 mg FeNC materials were suspended in 400 µL of liquid consisting of 200 µL of UP water, 150 µL isopropyl alcohol and 50 µL Nafion. The mixed liquid was homogenized by ultrasound for 30 min. The catalyst ink was then drop casted on a polished glassy carbon electrode followed by drying in the air for one day.

Computational Framework

Density functional theory (DFT) calculations were performed using the Vienna Ab-initio simulation package (VASP) [2, 3]. The ion-electron interactions were described by the projector augmented wave potential [4]. General gradient approximation is used as the exchange and correlation functional parameterized by Perdew Burke, and Ernzerhof [5]. Plane-wave basis sets with an energy cutoff of 500 eV [6]. For structural relaxation, the force on each atom is converged below 0.01 eV $Å^{-1}$. To avoid periodic image interaction, a vacuum separation of 30 Å was used to isolate the system. For the absorption calculation, the supercells size of 17.0 Å × 19.7 Å × 27.2 Å

and a k-point mesh of 2 × 2 × 1 were used. Additional calculations with Van der Waals corrections of DFT-D3 method with Becke-Jonson damping [7] were performed to validate the current approach.

The adsorption energy is defined as

$$E_{ads} = E_{total} - E_{substrate} - E_{molecule}$$

where E_{total}, $E_{substrate}$, and $E_{molecule}$ denote the total energy of substrate with adsorbate, substrate, and free molecule, respectively.

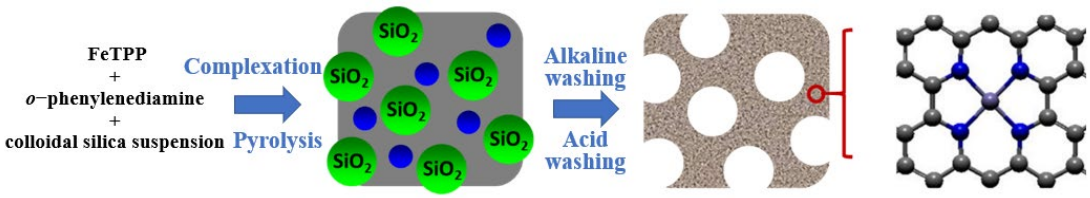

Figure S1. Schematic illustrations of FeNC nano sheets synthesis

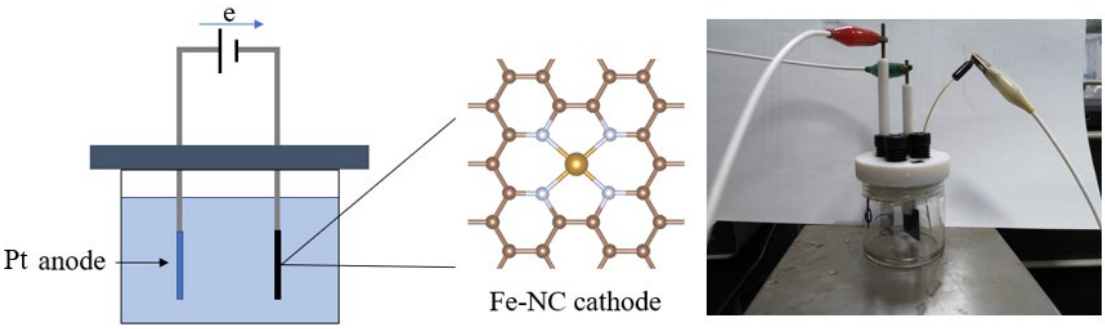

Figure S2. Schematic illustration and photo of electrochemical reactor.

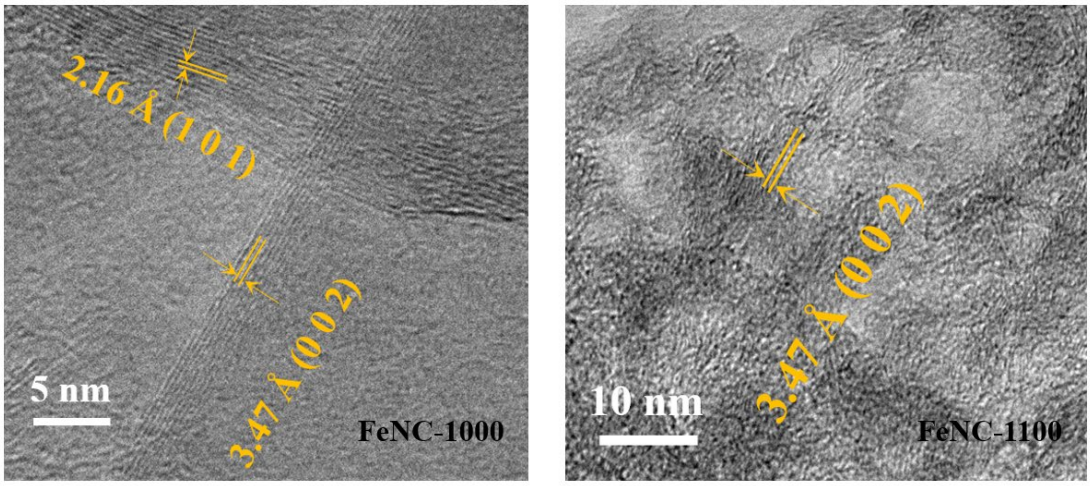

Figure S3. HRTEM image of FeNC-1000 and FeNC-1100

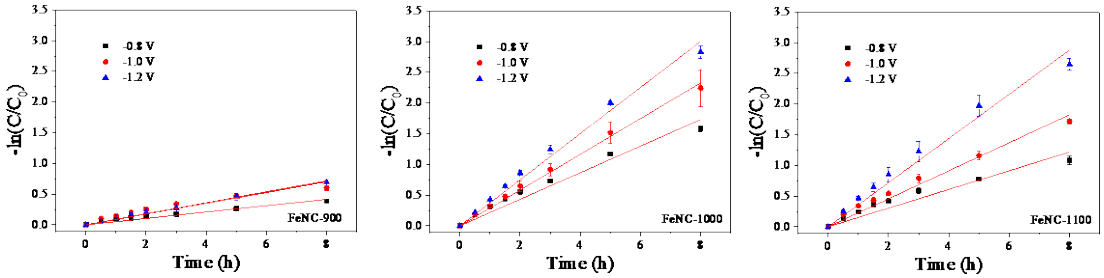

Figure S4. TCE removal rate constants at different potentials fitted by pseudo-first order kinetics. Reaction conditions: 2 mM Na_2SO_4 electrolyte; pH = 7.0; initial TCE concentration = 25 μM.

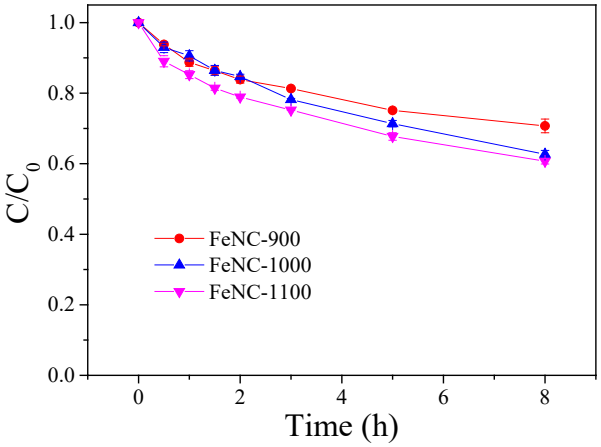

Figure S5. The adsorption of TCE by glassy carbon cathode and FeNC cathodes without applying potential. Reaction conditions: 2 mM Na_2SO_4 electrolyte; pH = 7.0; initial TCE concentration = 25 μM.

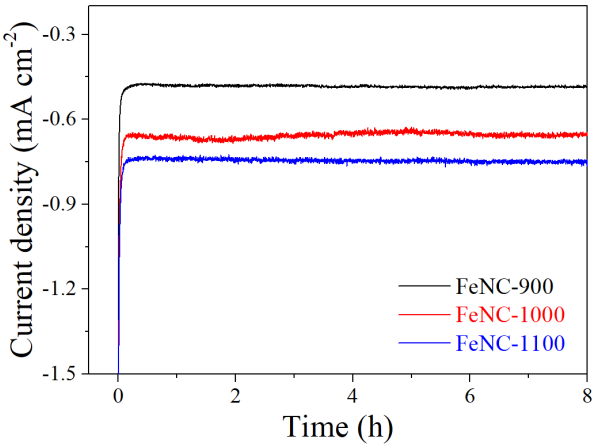

Figure S6. Change of current density during electrochemical reduction of TCE at −1.0 V. Reaction condition: electrolyte = 2 mM Na_2SO_4, pH = 7.0, initial TCE concentration = 25 μM.

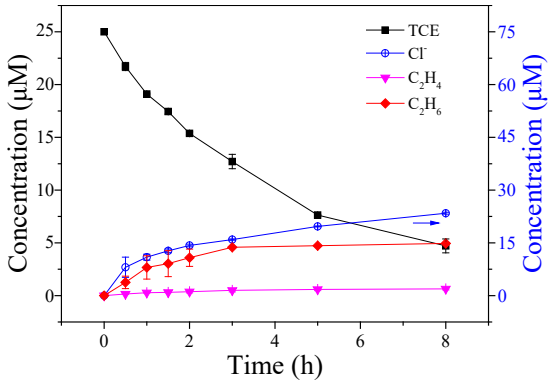

Figure S7. Dechlorination products of TCE using FeNC-1000 cathode with the presence of 100 mM TBA. Reaction condition: 2 mM Na_2SO_4 electrolyte, applied potential = −1.0 V, initial TCE concentration = 25 μM.

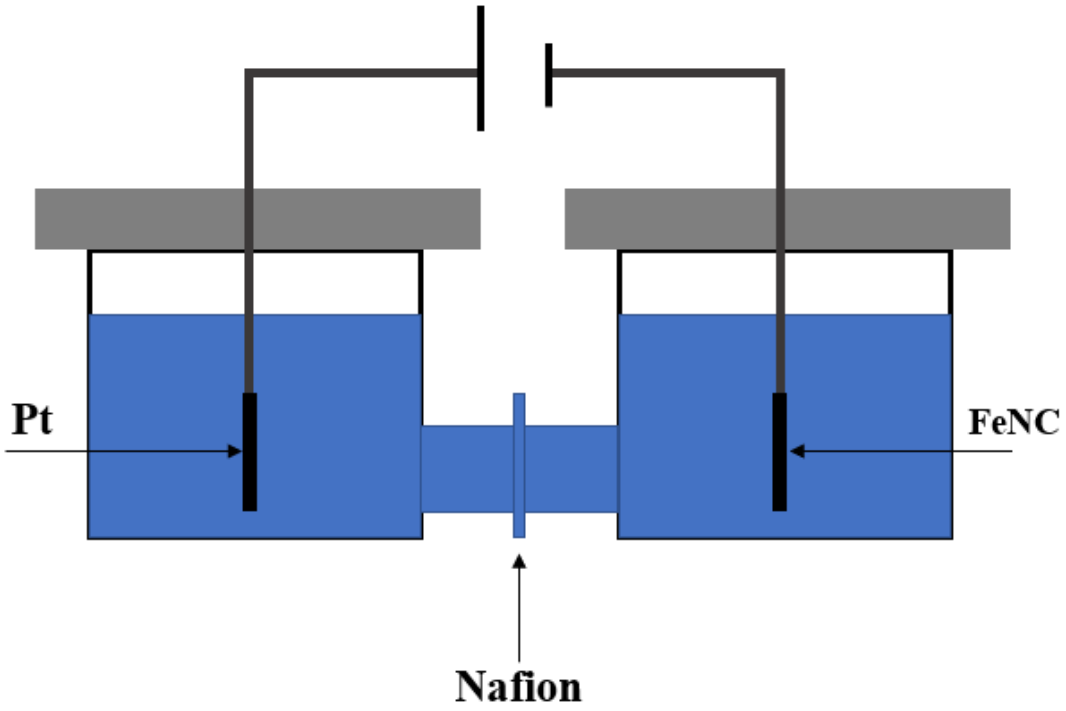

Figure S8. Schematic illustration of dual chamber electrochemical reactor. The volume of each chamber is 55 mL. The two chambers is separated by a Nafion ion exchange membrane.

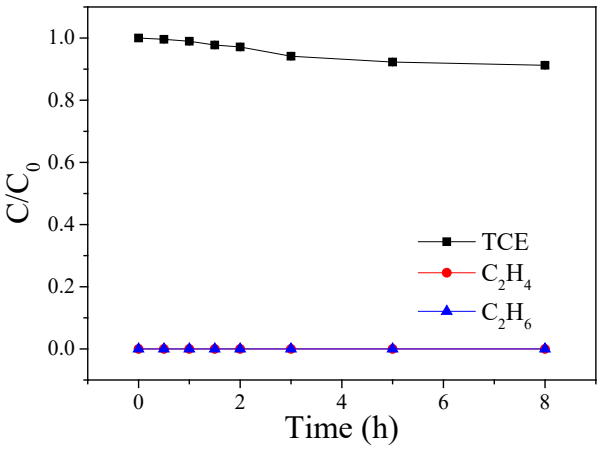

Figure S9. TCE removal and C_2H_4/C_2H_6 production in anodic chamber of the divided electrochemical cell. Reaction conditions: 2 mM Na_2SO_4 electrolyte, potential = –1.0 V, pH = 7.0, TCE initial concentration = 25 μM.

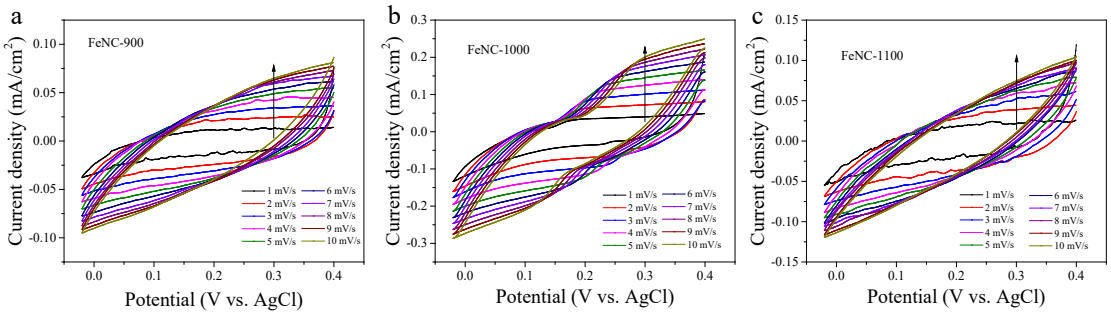

Figure S10. Electrochemically active surface area measurements for (a) FeNC-900, (b) FeNC-1000, and (c) FeNC-1100. Cyclic voltammograms taken in a potential range, in which no faradic processes were observed, to measure the capacitive current from double layer charging-discharging process.

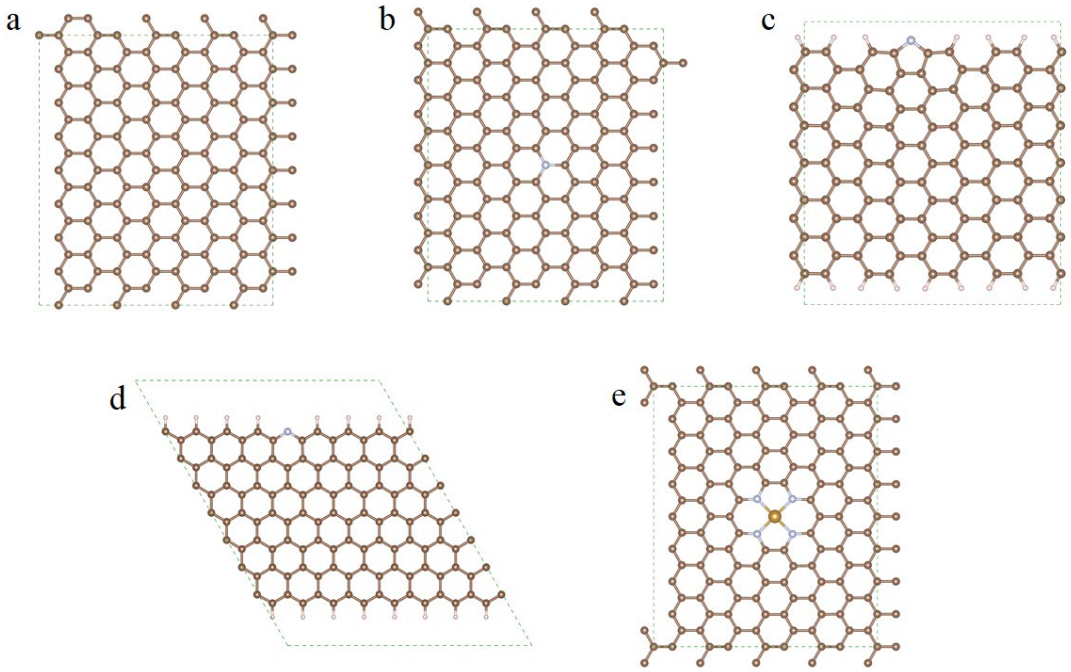

Figure S11. Optimized configuration of (a) graphene; (b) graphitic N doped graphene; (c) pyrrolic N doped graphene; (d) pyridinic N doped graphene and (e) Fe-N_4 structure of FeNC.

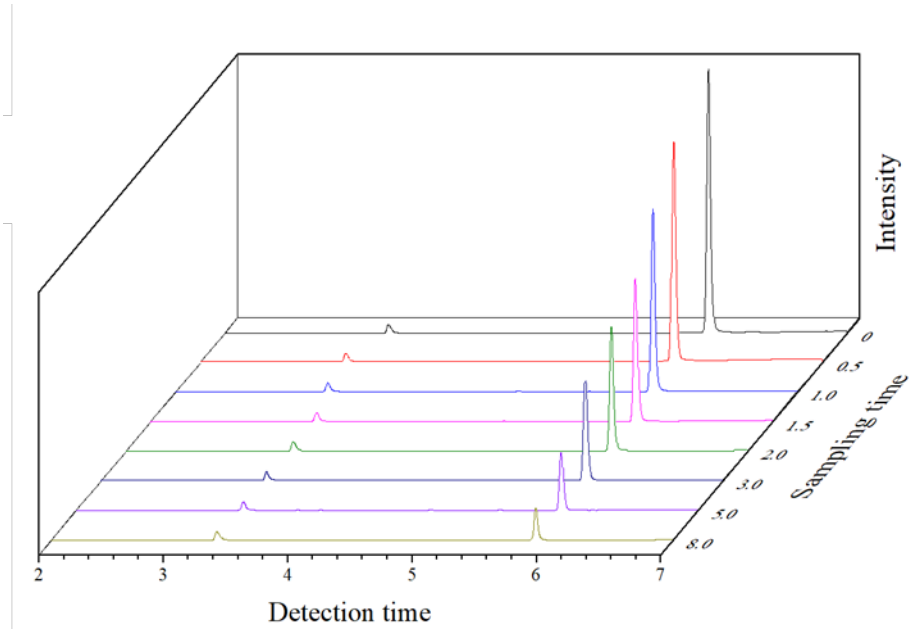

Figure S12. Change of gas chromatogram during TCE removal. The peak detected by GC-ECD at 6 minutes corresponded to TCE. The peak at 3.4 minutes resulted from air. Reaction condition: FeNC-1000 was used, applied potential = −1.0 V; electrolyte = 2 mM Na_2SO_4; pH = 7.0; initial TCE concentration = 25 μM.

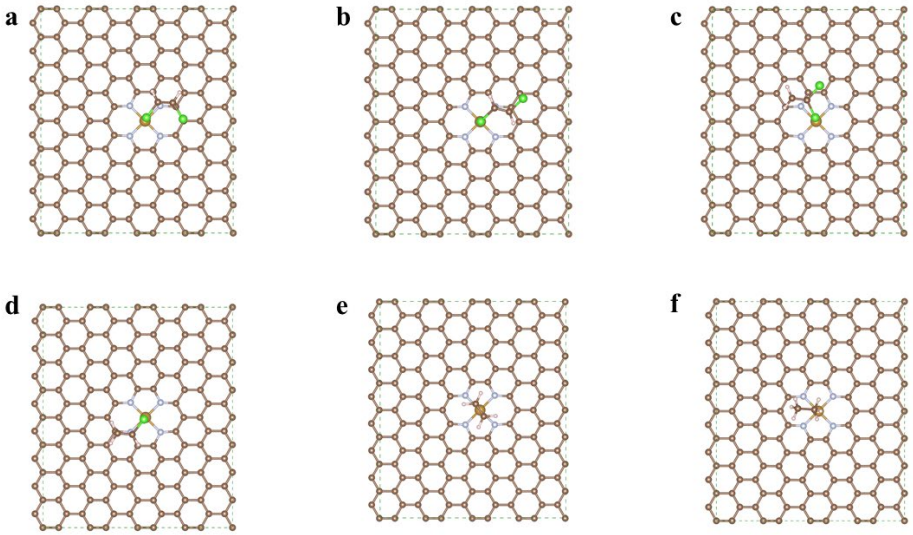

Figure S13. Optimized configuration of (a) FeNC + *cis*-DCE; (b) FeNC + *trans*-DCE; (c) FeNC + *1,1*-DCE; (d) FeNC + VC; (e) FeNC + ethylene and (f) FeNC + ethane.

Table S1. The composition of different forms of N in FeNC.

	Pyridinic N	Pyrrolic N	Graphitic N	Oxidized N
FeNC-900	31.2%	8.2%	58.5%	2.2%
FeNC-1000	22.6%	2.9%	65.8%	8.6%
FeNC-1100	9.9%	3.3%	73.6%	13.2%

Table S2. Adsorption energy between TCE with different forms N doped graphene.

Form	Adsorption energy (eV)
Graphene	0.05890874
Graphitic N doped graphene	0.05782459
Pyrrolic N doped graphene	0.0072696
Pyridinic N doped graphene	0.14527945
Fe-N_4 structure of FeNC	0.02889311

Table S3. Adsorption energy between FeNC with different dechlorination intermediates and products.

Form	Adsorption energy (eV)
FeNC + TCE	0.02889311
FeNC + *cis*-DCE	0.02341376
FeNC + *trans*-DCE	0.01831224
FeNC + *1,1*-DCE	0.02801792
FeNC + VC	-0.00925916
FeNC + ethylene	-0.12287453
FeNC + ethane	0.02566047

Table S4. Parameters of groundwater.

Parameters	pH	Cl^-	NO_3^-	SO_4^{2-}	TP	DO
Value	7.5	9.05	3.44	36.82	ND	6.92

Note: (1) the unit is mg L^{-1} excluding pH, (2) TP: total phosphorus, ND: not detected.

References

[1] H. Xin-Ming, H. Halvor HøEn, B.E. Tveden, D.K. Junker, M.M. Rohde, P. Marga-Martina, W. Edmund, L. Paolo, B.K. Birk, B. Martin, Selective CO_2 Reduction to CO in water using earth-abundant metal and nitrogen-doped carbon electrocatalysts, ACS Catalysis, 8 (2018) 6255-6264.

[2] G. Kresse, J. Hafner, Ab-initio molecular-dynamics simulation of the liquid-metal–amorphous-semiconductor transition in germanium, Physical Review B, 49 (1994) 14251-14269.

[3] G.G. Kresse, J.J. Furthmüller, Efficient iterative schemes for Ab Initio total-energy calculations using

a plane-wave basis set, Physical review. B, Condensed matter, 54 (1996) 11169-11186.
[4] P.E. Blochl, Projector augmented-wave method, Phys Rev B Condens Matter, 50 (1994) 17953-17979.
[5] J.P. Perdew, K. Burke, M. Ernzerhof, Generalized gradient approximation made simple, Physical Review Letters, 77 (1996) 3865-3868.
[6] H.J. Monkhorst, J.D. Pack, Special points for brillouin-zone integrations, Physical Review B, 13 (1976) 5188-5192.
[7] S. Grimme, J. Antony, S. Ehrlich, H. Krieg, A consistent and accurate ab initio parametrization of density functional dispersion correction (DFT-D) for the 94 elements H-Pu, Journal of Chemical Physics, 132 (2010) 154104.